Analysis of MS Progression with Hemisphere Histogram Comparison, Temporal Volumetric Analysis of Brain Regions, and Extraction of Brain Lesions through Marker-Controlled Watershed Algorithm

Alireza Banitalebidehkordi[1], Mohammad Mahdi Khalilzadeh[2], Farzan Khatib[3], Mahdi Azarnoosh[4]
1- Department of Biomedical Engineering, Mashhad Branch, Islamic Azad University, Mashhad, Iran.
Email: banitalebe@gmail.com
2- Department of Biomedical Engineering, Mashhad Branch, Islamic Azad University, Mashhad, Iran.
Email: mmkhalilzadeh@mshdiau.ac.ir(Corresponding author)
3- Department of Electrical Engineering, Mashhad Branch, Islamic Azad University, Mashhad, Iran.
4- Department of Biomedical Engineering, Mashhad Branch, Islamic Azad University, Mashhad, Iran.

Received: 14 March 2023 Revised: 27 May 2023 Accepted: 11 June 2023

ABSTRACT:
This paper proposes a novel method for rapidly and accurately detecting Multiple Sclerosis (MS) lesions and analyzing the progression of lesions and the disease based on differences between histograms of hemispheres and volumetric changes in brain regions over time. The brightness and contrast of pixels are first improved, and MRI slices are then analyzed to detect and eliminate the effects of motion artifacts while imaging. However, an accurate diagnosis tracks changes in volumes of brain regions caused by plaques emerging on brain MRIs in white matter, gray matter, and cerebrospinal fluid (CSF) and the concurrent analysis of differences between histograms of hemispheres. The marker-controlled watershed algorithm was employed to extract MS lesions and plaques. Various MRI centers differ in imaging diameters for which there are no unified standards, leading to different MRI slices. Hence, an individual's two MRI slices of two different occasions are not comparable. Measuring the brain volume can make the proposed method independent of the imaging diameter. This study analyzed the patients with at least three imaging records in the archives of imaging centers. The images were collected from Pars MRI Center and Hajar Hospital MRI Center in Shahrekord, Chararmahal and Bakhtiari Province, Iran. Both centers used Avanto MRI devices and performed imaging at 1 T and 1.5 T, respectively.

KEYWORDS: Multiple Sclerosis (MS), Volumetric Analysis of Brain Regions, Histograms of Hemispheres, Marker-Controlled Watershed Algorithm.

1. INTRODUCTION

Multiple Sclerosis (MS) is a destructively progressive neuro-inflammatory autoimmune disease caused by destroying protective covers (*i.e.*, myelin sheaths) around nerves. As a result, the brain will communicate with the other body parts with difficulty. However, the exact cause of MS is still unknown. Currently, the only treatment for MS includes rehabilitation and symptom management. There are some gray and white areas in the human brain MRI. The myelin-covered axons constitute the largest volume of this white matter, a great extent of which is destroyed in MS. Sclerosis or plaque refers to a wound. The disease is called multiple sclerosis because of emerging small or large numbers of wounds and plaques in different areas of the nervous system. The functions of nerves are damaged wherever these wounds emerge. A plaque can be as tiny as a needle or as large as a ping-pong ball. The lesions are diagnosed by doctors examining MRIs. T2-weighted (T2-W) MRIs were used in this study, where the brightest area indicates the cerebrospinal fluid (CSF), whereas the darkest area represents the white matter. Moreover, the gray matter is displayed by the average brightness, whereas lesions (*i.e.*, plaques) are shown as the average-to-high brightness. The center of gravity on an image and the line between the two hemispheres are first determined to eliminate the effects of motion

Paper type: Research paper
DOI: 10.30486/mjee.2023.1979427.1071
How to cite this paper: A.R. Banitalebidehkordi, M. M. Khalilzadeh, F. Khatib and M. Azarnoosh, **"Analysis of MS Progression with Hemisphere Histogram Comparison, Temporal Volumetric Analysis of Brain Regions, and Extraction of Brain Lesions through Marker-Controlled Watershed Algorithm"**, *Majlesi Journal of Electrical Engineering*, Vol. 17, No. 3, pp. 9-17, 2023.

artifacts while imaging and to separate the hemispheres. After separating the two hemispheres in all slices through accurate analysis and comparison of their histograms, the results are compared with healthy individuals' hemispheres. Their differences are then considered to determine the MS progression caused by the proliferation of brain plaques. Afterward, K-means and PCM algorithms are employed to distinguish white matter, gray matter, and CSF in all existing MRI slices without separating lesions from these three areas and by considering only three clusters. This process aims at tracking MS progression. The marker-controlled watershed algorithm is then adopted to extract lesions and plaques from all MRI slices and determine their 3D boundaries.

2. DESCRIPTION OF PAPER

Controlling a patient's head motions is considered a serious challenge in MRI. This challenge is much more important when patients have difficulty to keep their heads still for long. To detect and eliminate the effects of head motions while imaging, this paper employs the technique of finding and selecting the center of gravity and the longest diameter on the elliptical plane of each axial brain slice, i.e., the line separating the two hemispheres. Afterward, the two hemispheres are distinguished. Fig. 1 demonstrates some cases of head motions in MRI.

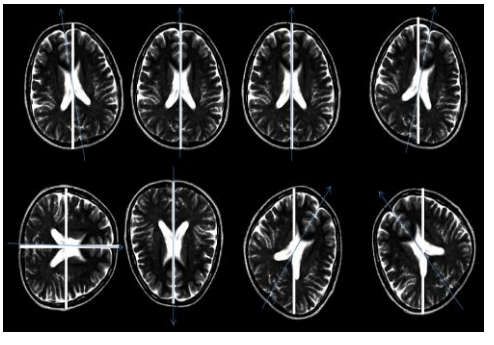

Fig. 1. Images of head motions in MRI.

The center-of-mass algorithm is adopted to find the brain's center, separate the two hemispheres, and eliminate motion artifacts. Each axial slice of an MRI is first binarized, and a mask of the brain image is then prepared. To this end, the designated MRI slice is binarized to eliminate its noise as much as possible. Afterward, a rectangle is placed on the MRI slice boundaries. The PCA algorithm is then utilized to extract the slice mask. It is now possible to distinguish between the right and left hemispheres by having the elliptical mask center through the mass algorithm and using its long diameter as the middle line of the brain. Fig. 2 illustrates different steps in extracting the designated slice mask from an MRI. The diameters are calculated by determining the intersection of each diameter passing through the ellipse center, and the longest diameter is selected as the middle line of the brain. "Ref. [25]"

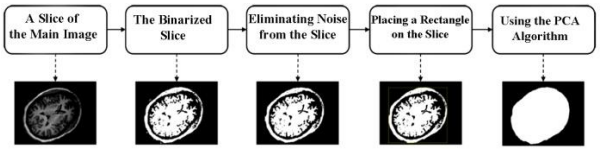

Fig. 2. Different steps in extracting the designated axial slice mask from an MRI.

By having the boundary line between the two hemispheres and comparing its angle with the vertical axis, it is possible to detect and modify any rotations or deviations of the head while imaging. This process is implemented on all axial slices of an MRI, as shown in Fig. 3.

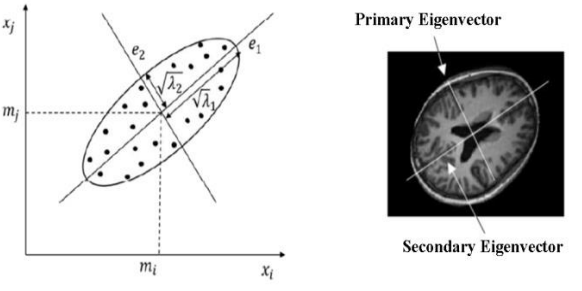

Fig. 3. The orthogonal eigenvector with the PCA: The left diagram indicates an eigenvector (e1) that represents the maximum variance through the center of the elliptical region and e2 that is perpendicular to e1. The right image depicts the eigenvectors extracted from brain MRIs and applied to images.

The histogram of each hemisphere is now drawn on all axial slices of a patient's MRI. The histograms of both hemispheres from each slice are then compared to extract their differences. This process determines how much the disease has affected each hemisphere and other parts of the body. Differences between the histograms of hemispheres can also be considered to pinpoint the potential locations of brain lesions. The corresponding histograms of a patient's previous MRIs are then compared to determine MS progression. When a patient is under treatment through specific medications prescribed by a doctor, the effects of treatment on his/her body can be analyzed. Fig. 1 demonstrates seven MRI slices taken from a 42-year-old woman with MS. The two hemispheres are distinguished in each slice.

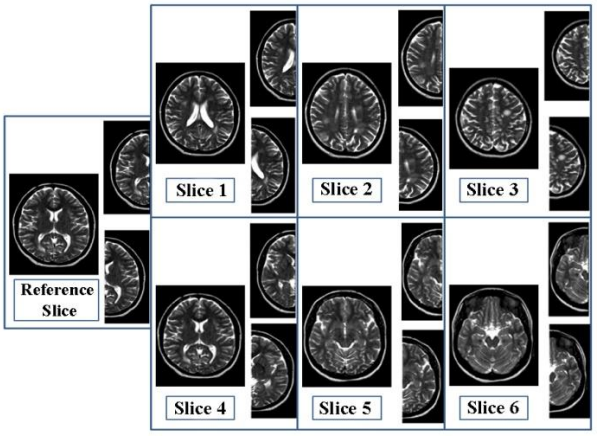

Fig. 4. Samples of axial T2-W MRI slices of the brain and separation of the two hemispheres for a patient with MS

The histogram of each slice is now obtained. The area under the histogram curve is deleted for better analysis, and only its envelope is drawn. Since the histograms of the human brain hemispheres are exactly symmetric, a difference between the two histograms can indicate the presence of a brain lesion or can only be caused by noise. The noise can be identified and eliminated through a more accurate comparison between points of difference in the histograms of hemispheres and the characteristics of noise and brain lesions. The remaining points will be the possible locations of brain lesions caused by MS. These lesions can be followed on all slices to extract their approximate 3D sizes. The participants in this study had at least three MRI records; thus, their other images can be monitored to analyze MS progression and its reaction to the treatment procedure. The following images (A, B, C, D, E, F, and G) demonstrate seven axial slices of MRIs taken from a patient with MS. The proposed method was employed to pinpoint the possible regions of MS lesions.

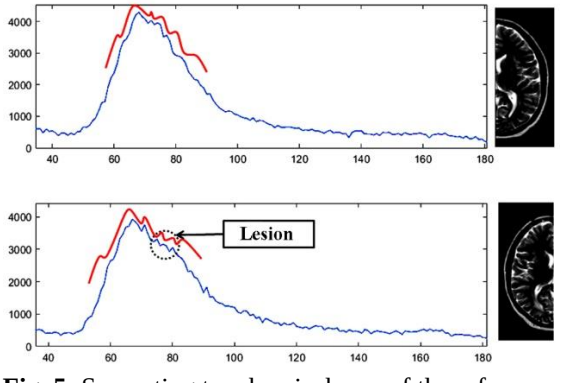

Fig. 5. Separating two hemispheres of the reference MRI slice and comparing their histograms from a patient with MS

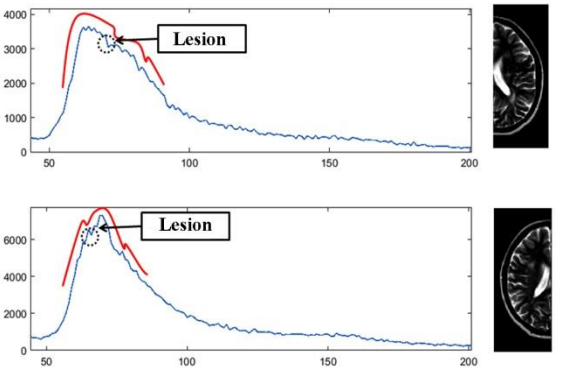

Fig. 6. Separating two hemispheres of MRI Slice 1 and comparing their histograms from a patient with MS

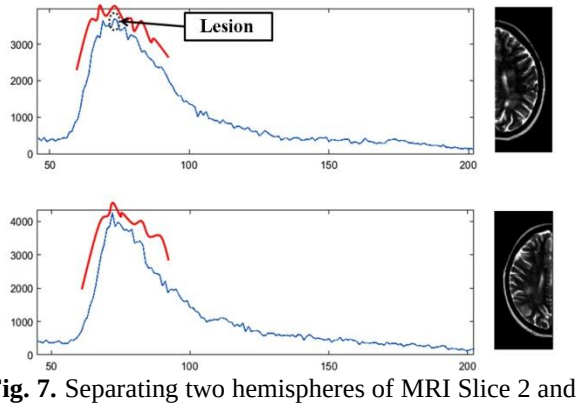

Fig. 7. Separating two hemispheres of MRI Slice 2 and comparing their histograms from a patient with MS

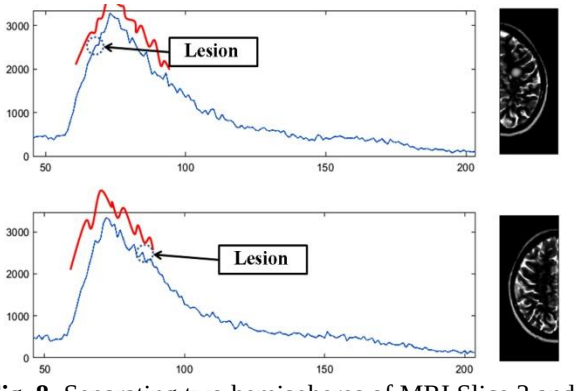

Fig. 8. Separating two hemispheres of MRI Slice 3 and comparing their histograms from a patient with MS

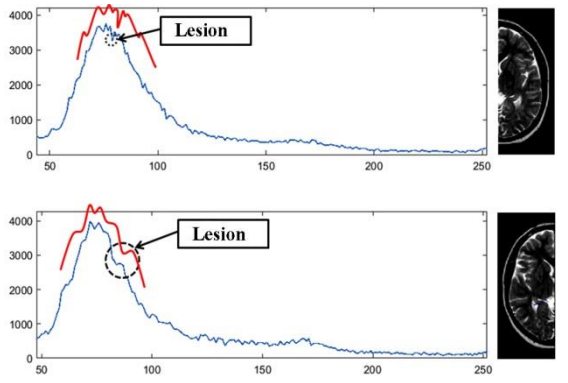

Fig. 9. Separating two hemispheres of MRI Slice 4 and comparing their histograms from a patient with MS

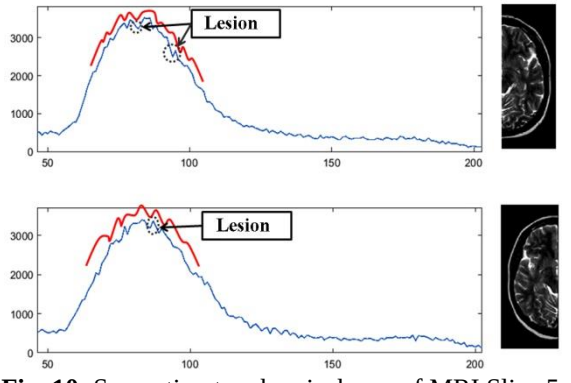

Fig. 10. Separating two hemispheres of MRI Slice 5 and comparing their histograms from a patient with MS

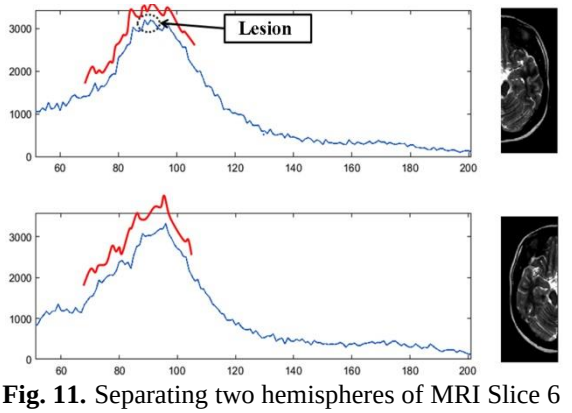

Fig. 11. Separating two hemispheres of MRI Slice 6 and comparing their histograms from a patient with MS

Four statistical measures, including mean, variance, standard deviation, and entropy, were employed to analyze and compare the histograms of hemispheres. Tables 1–4 present the results.

Table 1. The means of two MRIs from a patient with MS

Case 1 : 1395/09/14	mean	mean	Case 1 : 1397/08/14
Case 1 = Main	55.2648552699307	55.6776212832551	Case 1 = Main
Case 1 = Slice 1	62.3064955014264	56.9613830798479	Case 1 = Slice 1
Case 1 = Slice 2	58.4056822889857	56.2134467230903	Case 1 = Slice 2
Case 1 = Slice 3	60.9420435466009	53.601676701064	Case 1 = Slice 3
Case 1 = Slice 4	60.6429874869656	59.9770428457779	Case 1 = Slice 4
Case 1 = Slice 5	62.2113710887083	58.5971521777464	Case 1 = Slice 5
Case 1 = Slice 6	62.3840864263941	59.4567490494296	Case 1 = Slice 6

Table 2. The variances of two MRIs from a patient with MS

Case 1 : 1395/09/14	variance	variance	Case 1 : 1397/08/14
Case 1 = Main	2914.59165270989	2791.83174846006	Case 1 = Main
Case 1 = Slice 1	3201.63024839414	2942.37558499115	Case 1 = Slice 1
Case 1 = Slice 2	3025.97089478627	2641.21145458364	Case 1 = Slice 2
Case 1 = Slice 3	3228.42866487065	2715.95055247628	Case 1 = Slice 3
Case 1 = Slice 4	2905.59752243576	2825.88571441274	Case 1 = Slice 4
Case 1 = Slice 5	2939.633100185	2647.52370599361	Case 1 = Slice 5
Case 1 = Slice 6	3270.52352913893	2683.56543560654	Case 1 = Slice 6

Table 3. The standard deviations of two MRIs from a patient with MS

Case 1 : 1395/09/14	Standard Deviation	Standard Deviation	Case 1 : 1397/08/14
Case 1 = Main	53.9869	52.8377	Case 1 = Main
Case 1 = Slice 1	56.58295	54.2436	Case 1 = Slice 1
Case 1 = Slice 2	55.0088	51.3927	Case 1 = Slice 2
Case 1 = Slice 3	56.8192	52.1147	Case 1 = Slice 3
Case 1 = Slice 4	53.90359	53.159	Case 1 = Slice 4
Case 1 = Slice 5	54.2183	51.454	Case 1 = Slice 5
Case 1 = Slice 6	57.1885	51.8031	Case 1 = Slice 6

Table 4. The entropies of two MRIs from a patient with MS

Case 1 : 1395/09/14	Entropy	Entropy	Case 1 : 1397/08/14
Case 1 = Main	6.16680232236052	6.27187809686649	Case 1 = Main
Case 1 = Slice 1	6.3742794640794	6.22537375733737	Case 1 = Slice 1
Case 1 = Slice 2	6.21816059075535	6.23017270896023	Case 1 = Slice 2
Case 1 = Slice 3	6.26799469189563	6.09690345094427	Case 1 = Slice 3
Case 1 = Slice 4	6.45447837354524	6.4372692587568	Case 1 = Slice 4
Case 1 = Slice 5	6.80351387922309	6.42272550350627	Case 1 = Slice 5
Case 1 = Slice 6	6.75453856102517	6.52570275352941	Case 1 = Slice 6

Tables 1 to 4 show the means, variances, standard deviations, and entropies of corresponding slices in the two MRIs captured by Avanto at 1.5 T. It is possible to compare changes in the disease over time and pursue its progression. It is also essential to analyze volumetric changes of brain regions caused by plaques in white matter, gray matter, and CSF on MRIs to better determine disease progression.

3. VOLUMETRIC ANALYSIS

Considering the serious effects of the noise and heterogeneity of images on the non-brain tissues such

as the skull and fat, it is advisable to remove the non-brain tissues to reduce the computation time and improve the efficiency of processing steps. Hence, the brain is first separated from the background, and the skull is removed from the image. The skull appears very bright on T2-W MRIs of the brain. Hence, the histograms of nonblack points are extracted from the primary image and are then used along with an appropriate threshold to first extract and remove only the skull from an MRI. Fig. 12 demonstrates an MS patient's skull removed from the middle axial slice of a T2-W brain MRI through the proposed method. "Ref. [24],[27]"

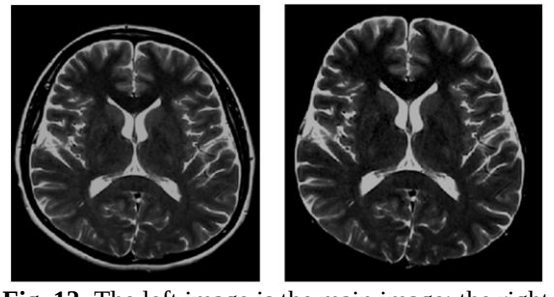

Fig. 12. The left image is the main image; the right image is the main image without the skull.

Separating MS plaques on T2-W MRIs would be very similar to the brain tissue and CSF; therefore, separation plaques will not always be correctly detectable and can be prone to a high error level. Hence, we do not intend to remove plaques from white matter, gray matter, and CSF to analyze changes and progression over time. Instead, we would like to consider plaques among those regions and measure the progression in each hemisphere and the entire brain tissue by analyzing the volumetric changes of those three regions and the changes in plaques. Since plaques are naturally the inflammation of demyelination, they are mainly detected as CSF and WM on T2-W MRIs while image segmentation. They change the areas of brain regions in each slice and finally change the volumes of regions in the entire brain tissue. If inflammation declines, the volumes of regions will proportionately change again. By analyzing these changes, it is possible to predict the future behavior, type, and progression of MS. To this end, we decided to select patients with at least three MRIs over time. The designated MRIs were taken from 20-70-year-old men and women.

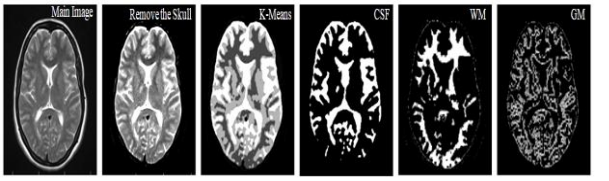

Fig. 13. (A): An MRI slice from an MS patient; (B): Improving resolution and brightness and separating the skull from the image; (C): Using the K-means algorithm with three clusters to separate three brain regions; (D) Separating CSF; (E): Separating WM; (F): Separating GM.

In the next step, the GM, WM, and CSF regions should be separated on a skull-free MRI to calculate the volume of each brain region. For this purpose, we use a combinatorial method of setting a brightness threshold with the image histogram and improving brightness and resolution. After that, the K-means algorithm is employed to better segment brain images based on the brain MRI slice type. Finally, the FCM algorithm is adopted to separate the segmented regions. Fig. 13 illustrates the steps of this process.

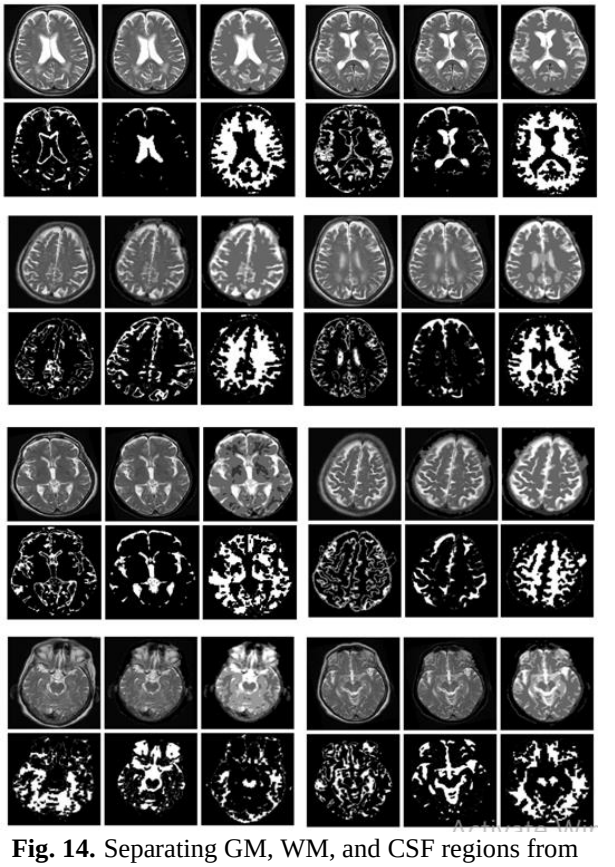

Fig. 14. Separating GM, WM, and CSF regions from MRI slices of an MS patient

The brain regions were separated, and the area of each region (i.e., GM, WM, and CSF) was calculated in

each slice. Since slices differ in diameter and area, they affect the total brain volume differently. Therefore, the middle slice with the longest diameter should be selected as the reference slice, and a coefficient should proportionately be extracted for other slices to determine their effects on the total brain volume. The areas of GM, WM, and CSF regions are then multiplied by the corresponding coefficients of slices. The resultant products are then added to calculate the volumes of GM, WM, and CSF regions in percentage. In Fig. 14, this process was applied to all MRI slices. "Ref. [22],[27]"

In this method, a patient's brain volume is obtained from his/her MRI independently of other patients' MRIs. The volume of each region is expressed as a percentage of the total brain volume. This method can be applied to all images regardless of the imaging diameter. However, the shorter the imaging diameter with further slices, the higher the accuracy of calculating the volumes of regions. Table 1 reports the evaluation results of a 50-year-old woman with three brain MRIs at the MRI Center of Hajar Hospital in Shahrekord. She underwent the second imaging process seven months after the first imaging process. She underwent the third imaging process four months after the second. Imaging was performed on all three occasions on Avanto with a power of 1.5 T and a diameter of 5 mm. The means, variances, standard deviations, and entropies of images were measured to compare the results.

Table 5. Volumetric changes of GM, CSF, and WM regions in three MRI process and observation of progression.

The 50-year-old female patient in the first MRI process	GM	CSF	WM
July 16, 2016	57.446%	22.701%	19.852%
February 9, 2017	44.818%	26.108%	29.073%
June 8, 2017	44.182%	26.323%	29.494%

Since the inflammations of demyelination around axons have bright surfaces on T2-W MRIs of the brain, they can be detected as parts of CSF or WM. Therefore, we expect to be able to determine MS progression by following the volumetric changes of these two regions and analyzing the volumetric changes of another brain region on MRIs captured from a patient over time. Hence, we can take more effective steps in providing treatment and predicting the type and severity of future complications. According to the results, the 50-year-old female patient experienced progressing changes in CSF during the one year of MS, indicating the increasing problems caused by the growth and multiplicity of MS-caused plaques. Hence, her progression can be predicted as the primary progressive MS (PPMS), which was also confirmed in the follow-up performed by her doctor. Thus, the results were accurate.

Table 6. Comparing the volumes of GM, CSF, and WM regions in mean, variance, entropy, and standard deviation in three MRI processes for Progression observation.

The 50-year-old female patient in the first MRI process	Entropy	SD	Mean	Variance
July 16, 2016	6.3775	52.4263	60.9141	2750.8
February 9, 2017	6.4536	52.4868	65.5911	2755.4
June 8, 2017	6.7836	52.5171	71.0756	2763.94

Table 6 presents the results of statistical measures such as entropy, standard deviation, mean, and variance, which confirmed the research findings.

4. EXTRACTION OF BRAIN LESIONS AND PLAQUES

The marker-controlled watershed transform was employed in the final step of MS diagnosis to extract lesions and plaques from MRIs. The watershed transform uses the gradient domain of an image as the target surface. The pixels with the longest gradient domains on an MRI are mapped onto the watershed lines representing the boundaries of regions. In the marker-controlled watershed algorithm, segmentation rules are based on a marker for converting an input image so that the algorithm can indicate the similarities of objects on the converted image. The markers represent the components of an image and are utilized to prevent excessive segmentation in the watershed segmentation method. The internal markers depend on the objects of interest inside an image, whereas the external markers depend on the background. After segmentation, the boundaries of watershed regions are placed on the favorable edges; hence, each object is separated from its neighboring objects. Integrating morphology operators (e.g., opening and closing) on an image and then image reconstructing in each step can eliminate the tiny components of an image much more efficiently than the conventional standard method. It can also mitigate the redundancy effect; therefore, the excessive tiny regions are removed from the image in two steps (i.e., application of an opening operator and image reconstruction in the first step and application of opening-closing operators and reconstruction in the second step). Similarly, the small discrete regions are connected to improve the image quality, select the

favorable markers, and segment regions with high accuracy. According to the marker-controlled watershed algorithm (Fig. 15), this method resolved most of the complications and limitations in conventional methods. "Ref. [11],[19]"

Fig. 15. The block diagram of the proposed marker-controlled watershed transform algorithm for brain MRI segmentation

The resultant foreground marker image was placed on the main image to better interpret the segmentation results. Adding this image to the main image will highlight the regions and improve segmentation. Since some closed regions were not marked in the image segmentation, they will not be segmented correctly in the final segmentation results. Moreover, the foreground markers move toward an objects' edge in some cases. The bubble and thick edges of markers should be modified and smoothed to resolve these two problems. They should then be made slightly smaller. To this end, the closing operator is first applied to the image. After that, the erosion operator is used. In the next step, the background markers of the image should be marked. Since dark pixels belong to the background on these images, the background markers can be extracted by placing an image's correct threshold and selecting dark pixels. Although the background pixels should logically be black pixels, the background is made thin towards the foreground as much as possible through the SKIZ technique because it is not preferable to keep background markers very close to the segmentation candidate objects in an ideal case. This process is performed through the watershed transform by calculating the distances of edge lines extracted from the foreground using the same transform.

5. EXPERIMENTAL RESULTS

Fig. 16 compares the segmentation results of the marker-controlled watershed algorithm in the proposed method on MRIs with those of a conventional algorithm. According to the results, the marker-controlled image in the proposed method overcame excessive segmentation. Fig. 16(a) depicts an MRI selected randomly from the test samples. According to Fig. 16(b), a gradient was first applied to the selected sample to determine the image minimum at each gray level. The resultant minimums can be considered as appropriate markers for applying the watershed transform to the image. The watershed lines start expanding from those minimums. Hence, Fig. 16(c) indicates the result of using this idea through the watershed transform on the gradient domain. Since MRIs are prone to various noises of Gaussian, Poison, rail, and pulse (pepper-salt) types, it is essential to use noise reduction and elimination methods to improve the quality of these images for better diagnose of diseases. In the next step, morphology operators are employed to reduce noise and improve image quality as much as possible. Fig.16(d) demonstrates opening operations in one step, where some narrow paths are disconnected and broken down, or the tiny bumps caused by fluctuations, and nonlinear effects are removed from the image. The combinatorial opening-closing operations are then performed to further reduce and remove noise. Fig. 16(g) shows the outputs of these operations. As a result, the effects of noise remaining on the edges and margins of the thin edges of the image will greatly be reduced, and the resultant image will have nearly no noise on its edges, which are separable.

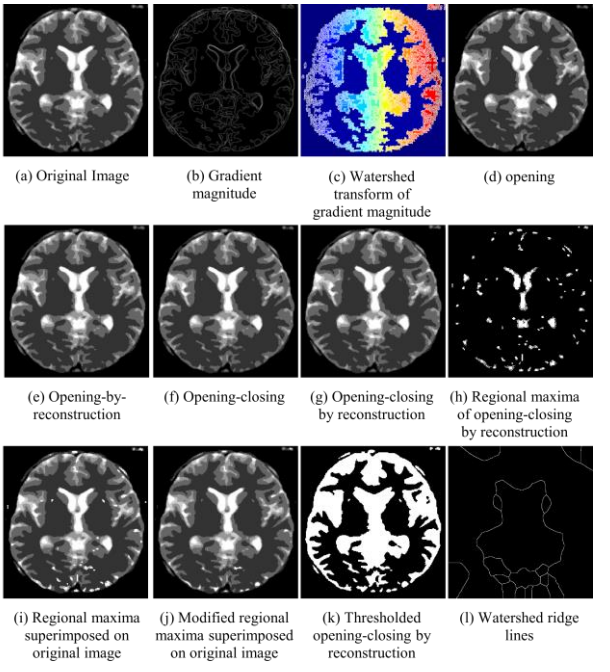

Fig 16: The results of implementing the proposed method on the exclusive images taken from Pars Clinic and Hajar Hospital of Shahrekord: (a) The main image; (b) Gradient on the domain; (c) The watershed transform on the domain gradient; (d) opening; (e) Image reconstruction after opening; (f) Image reconstruction after application of opening; (g) Opening and closing (LOC); (h) Edge lines of image regions after application of the watershed algorithm; (i) Local maximum from opening-closing through image reconstruction (fgm); (j) Adding local maximums to the main image; (k) Reconstruction by placing a threshold on opening and closing; (l) Edge lines of the image watershed Conclusion

According to Fig. 16(g), a binary image is created

by placing a threshold on the reconstructed image obtained from opening-closing operations. After the watershed algorithm was adopted, it was easy to determine the image edge lines on which excessive segmentation was dealt with. According to Fig. 16(h), it is possible to follow the regions segmented in the marker-controlled watershed algorithm by adding local maximums to the main image. The regions can be highlighted in different colors for better visual detection. Although the number of iterations decreased in this algorithm, the runtime remained constant. In each iteration, the elapsed time prolongs as expected by only increasing the number of markers. This algorithm requires a reasonable amount of memory. If a normal distribution is considered for markers on the image regions, it will be possible to estimate the number of points belonging to each watershed region. "Ref. [1],[5].

The center-of-mass algorithm was used to find the center of the brain. An appropriate threshold was selected in the PCA algorithm to create an elliptical mask of a brain MRI on which the long diameter was considered the middle line of the brain. "Ref. [32],[34]" The histograms of the right and left hemispheres were then extracted using the line between the two hemispheres. The means and variances of all existing MRI slices were then obtained and compared to find the possible differences caused by lesions and plaques in MS. Since the visual observation by doctors to reach a diagnosis, especially in the early stages of a disease, cannot be accurate enough and would also be based on a doctor's competence and experience; the proposed method can be efficient in making a faster diagnosis. This method was implemented on 56 patients, and the resultant accuracy was more than 98%, indicating its satisfactory performance. The temporal volumetric analysis of brain regions was also used along with the proposed method to improve the accuracy of results up to 100%. The results of the volumetric analysis also diagnosed the type of MS from which the designated case suffered. This method was evaluated on all types of MS: primary progressive MS (PPMS), relapsing remitting MS (RRMS), progressive-relapsing MS (PRMS), and secondary progressive MS (SPMS). The tests were conducted on 56 patients who had undergone at least three brain MRI processes at either Hajar Hospital MRI Center or Pars MRI Center in Shahrekord. The results of diagnoses and MS types of patients were consistent with the medical diagnoses made by doctors. Hence, it can be concluded that the calculation accuracy was 100% on the evaluated patients, indicating this method's high accuracy. Finally, the marker-controlled watershed algorithm was employed to extract lesions and plaques and analyze their changes to evaluate MS progression.

REFERENCES

[1] S. Chawla, I. Kister, T. Sinnecker, J. Wuerfel, J.-C. Brisset, F. Paul et al., "**Longitudinal study of multiple sclerosis lesions using ultrahigh field (7T) multiparametric MR imaging**", **PLoS One**, Vol. 13, pp. e0202918, 2018.

[2] D. R. Nayak, R. Dash, B. Majhi and V. Prasad, "**Automated pathological brain detection system: A fast discrete curvelet transform and probabilistic neural network based approach**", *Expert Systems with Applications*, Vol. 88, pp. 152-164, 2017.

[3] T. Frisch, M. L. Elkjaer, R. Reynolds, T. M. Michel, T. Kacprowski, M. Burton et al., "**Multiple sclerosis atlas: A molecular map of brain lesion stages in progressive multiple sclerosis**", *Network and systems medicine*, Vol. 3, pp. 122-129, 2020.

[4] H. Kim, E. Shim, J. Park, Y.-J. Kim, U. Lee and Y. Kim, "**Web-based fully automated cephalometric analysis by deep learning**", *Computer methods and programs in biomedicine*, Vol. 194, pp. 105513, 2020.

[5] R. McKinley, R. Wepfer, L. Grunder, F. Aschwanden, T. Fischer, C. Friedli et al., "**Automatic detection of lesion load change in Multiple Sclerosis using convolutional neural networks with segmentation confidence**", *NeuroImage: Clinical*, Vol. 25, pp. 102104, 2020.

[6] R. Pourreza, Y. Zhuge, H. Ning, and R. Miller, "**Brain Tumor Segmentation in MRI Scan Using Deeply-Supervised Neural Networks**," *brainless, Lect. Notes Comput. Sci*., Vol. 10670, pp. 320–331, 2018.

[7] Y. Li, F. Jia, and J. Qin, "**Brain Tumor Segmentation from Multimodal Magnetic Resonance Images via Sparse Representation**," *Artif. Intell. Med*.,Vol. 73, pp. 1–13, 2016.

[8] A. Ahmadvand, M. R. Daliri, and S. M. Zahiri, "**Segmentation of Brain MR Images using a Proper Combination of DCS based method with MRF**," *Multimedia. Tools Appl*., Vol. 77, no. 7, pp. 8001–8018, 2018.

[9] G. Wang et al., "**Interactive Medical Image Segmentation Using Deep Learning with Image-Specific Fine Tuning,**" *IEEE Trans. Med. Imaging*, Vol. 37, No. 7, pp. 1562–1573, 2018.

[10] J. Amin, M. Sharif, M. Yasmin, and S. L. Fernandes, "**A Distinctive Approach in Brain Tumor Detection and Classification using MRI**," *Pattern Recognit. Lett.*, pp. 1–10, 2017.

[11] S. M. K. Hasan and M. Ahmad, "**Two-Step Verification of Brain Tumor Segmentation using Watershed-Matching Algorithm,**" *Brain Informatics*, Vol. 5, 2018.

[12] E. Kats, J. Goldberger and H. Greenspan, "**Soft labeling by distilling anatomical knowledge for improved ms lesion segmentation,**", 2019 IEEE 16th *International Symposium on Biomedical Imaging (ISBI 2019)*, pp. 1563-1566, 2019.

[13] P. Narayana, I. Coronado, S. Sujit, J. Wolinsky, F. Lublin and R. Gabr, "**Deep learning for predicting enhancing lesions in multiple sclerosis from noncontrast mri,**", *Radiology*, Vol. 294, pp. 191, Dec. 2019.

[14] F. La Rosa, A. Abdulkadir, M. Fartaria, R. Rahmanzadeh, P.-J. Lu, R. Gal-busera, et al., "**Multiple sclerosis cortical and wm lesion segmentation at 3t mri: A deep learning method based on flair and mp2rage**,", *NeuroImage: Clinical*, Vol. 27, pp. 102, Jun. 2020.

[15] Christoph Baur, Benedikt Wiestler, Shadi Albarqouni and Nassir Navab, "**Fusing Unsupervised and Supervised Deep Learning for White Matter Lesion Segmentation,**", *Proceedings of Machine Learning Research*, Vol. 102, pp. 63-72, 2019.

[16] L. de Santiago, E. Sánchez Morla, M. Ortiz, E. López, C. Amo Usanos, M. Alonso-Rodríguez et al., "**A computer-aided diagnosis of multiple sclerosis based on mfVEP recordings**,", *PloS one*, Vol. 14, pp. e0214662, 2019.

[17] S. L. Jui et al., "**Brain MRI Tumor Segmentation with 3D Intracranial Structure Deformation Features,**" *IEEE Intell. Syst*., Vol. 31, No. 2, pp. 66–76, 2016.

[18] A. Lakshmi, T. Arivoli, and M. P. Rajasekaran, "**A Novel M-ACABased Tumor Segmentation and DAPP Feature Extraction with PPCSO-PKC-Based MRI Classification,**" *Arab. J. Sci. Eng*., pp. 1–17, 2017.

[19] A. Bieniek and A. Moga, "**An efficient watershed algorithm based on connected components**," ,*Pattern Recognition*, Vol. 33, No. 6, pp. 907–916, 2000.

[20] F. Meyer, "**Levelings and morphological segmentation**," *in Proceedings of SIBGRAPI'98, (Rio de Janeiro, Brazil)*, pp. 28–35, 1998.

[21] E. Roura, A. Oliver, M. Cabezas, S. Valverde, D. Pareto, J. Vilanova, L. Rami_o-Torrent_a, A. Rovira, and X. Llad_o, "**A toolbox for multiple sclerosis lesion segmentation**," *Neuroradiology*, Vol. 57, No. 10, pp. 1031–1043, 2015.

[22] M. Cabezas, A. Oliver, E. Roura, J. Freixenet, J. C. Vilanova, L. Rami_o-Torrent_a,_A. Rovira, and X. Llad_o, "**Automatic multiple sclerosis lesion detection in brain mri by air thresholding**," *Computer Methods and Programs in Biomedicine*, Vol. 115, No. 3, pp. 147–161, 2014.

[23] A. H. Zhuang, D. J. Valentino, and A. W. Toga, "**Skull-stripping magnetic resonance brain images using a model-based level set**," *NeuroImage*, Vol. 32, nNo. 1, pp. 79–92, 2006.

[24] J. G. Park and C. Lee, "**Skull stripping based on region growing for magnetic resonance brain images**," *NeuroImage*, Vol. 47, No. 4, pp. 1394–1407, 2009.

[25] K. Somasundaram and T. Kalaiselvi, "**Fully automatic brain extraction algorithm for axial T2-weighted magnetic resonance images**," *Computers in Biology and Medicine*, Vol. 40, No. 10, pp. 811–822, 2010.

[26] A. G. R. Balan, A. J. M. Traina, M. X. Ribeiro, P. M. A. Marques, and C. Traina Jr, "**Smart histogram analysis applied to the skull-stripping problem in T1-weighted MRI**,", *Computers in Biology and Medicine*, Vol. 42, No. 5, pp. 509–522, 2012.

[27] Y. Diez, A. Oliver, M. Cabezas, S. Valverde, R. Mart_, J. Vilanova, L. Rami_o-Torrent_a, _A. Rovira, and X. Llad_o, "**Intensity based methods for brain mri longitudinal registration. a study on multiple sclerosis patients,**", *Neuroinformatics*, Vol. 12, No. 3, pp. 365–379, 2014.

[28] E. Roura, T. Schneider, M. Modat, P. Daga, N. Muhlert, D. Chard, S. Ourselin, X. Llad_o, and C. A. M. Wheeler-Kingshott, "**Multi-channel registration of fa and t1w images in the presence of atrophy: application to multiple sclerosis**,", *Functional Neurology*, Vol. 30, No. 4, 2015.

[29] J. de Bresser, M. P. Portegies, A. Leemans, G. J. Biessels, L. J. Kappelle, and M. A. Viergever, "**A comparison of fMRg based segmentation methods for measuring brain atrophy progression**,", *NeuroImage*, Vol. 54, No. 2, pp. 760–768, 2011.

[30] V. Popescu, N. Ran, F. Barkhof, D. Chard, C. Wheeler-Kingshott, and H. Vrenken, "**Accurate fGMg atrophy quanti_cation in fMSg using lesion-_lling with coregistered 2d lesion masks**,", *NeuroImage: Clinical*, Vol. 4, pp. 366–373, 2014.

[31] Y. Wu, S. K. War_eld, I. L. Tan, W. M. W. III, D. S. Meier, R. A. van Schijndel, F. Barkhof, and C. R. Guttmann, "**Automated segmentation of multiple sclerosis lesion subtypes with multichannel fMRIg**,", *NeuroImage*, Vol. 32, No. 3, pp. 1205–1215, 2006.

[32] D. Garcia-Lorenzo, S. Prima, D. Arnold, D. Collins, and C. Barillot, "**Trimmedlikelihood estimation for focal lesions and tissue segmentation in multisequence mri for multiple sclerosis**,", *Medical Imaging, IEEE Transactions on*, Vol. 30, No. 8, pp. 1455–1467, 2011.

[33] M. Battaglini, M. Jenkinson, and N. De Stefano, "**Evaluating and reducing the impact of white matter lesions on brain volume measurements**,", *Human Brain Map- ping*, Vol. 33, No. 9, pp. 2062–2071, 2012.

[34] M. Sdika and D. Pelletier, "**Nonrigid registration of multiple sclerosis brain images using lesion inpainting for morphometry or lesion mapping**,", *Human Brain Mapping*, Vol. 30, No. 4, pp. 1060–1067, 2009.